IOPscience iopscience.iop.org

Home Search Collections Journals About Contact us My IOPscience

Water-window soft x-ray high-harmonic generation up to the nitrogen K-edge driven by a kHz, 2.1 m OPCPA source

This content has been downloaded from IOPscience. Please scroll down to see the full text.

2016 J. Phys. B: At. Mol. Opt. Phys. 49 155601

(http://iopscience.iop.org/0953-4075/49/15/155601)

View the table of contents for this issue, or go to the journal homepage for more

Download details:

IP Address: 131.169.239.204
This content was downloaded on 02/08/2016 at 10:57

Please note that terms and conditions apply.

OPEN ACCESS
IOP Publishing
Journal of Physics B: Atomic, Molecular and Optical Physics
J. Phys. B: At. Mol. Opt. Phys. **49** (2016) 155601 (8pp)
doi:10.1088/0953-4075/49/15/155601

Water-window soft x-ray high-harmonic generation up to the nitrogen K-edge driven by a kHz, 2.1 μm OPCPA source

Gregory J Stein[1,5], Phillip D Keathley[1,5], Peter Krogen[1], Houkun Liang[1], Jonathas P Siqueira[1,2], Chun-Lin Chang[1], Chien-Jen Lai[1], Kyung-Han Hong[1], Guillaume M Laurent[1] and Franz X Kärtner[1,3,4]

[1] Department of Electrical Engineering and Computer Science and Research Laboratory of Electronics, Massachusetts Institute of Technology, Cambridge, MA 02139, USA
[2] Grupo de Fotônica, Instituto de Fsica de São Carlos, Universidade de São Paulo, SP 13560-970, Brazil
[3] Center for Free-Electron Laser Science, DESY and Department of Physics, University of Hamburg, Hamburg, Germany
[4] The Hamburg Center for Ultrafast Imaging, Luruper Chaussee 149, D-22761 Hamburg, Germany

E-mail: kaertner@mit.edu

Received 4 April 2016, revised 18 May 2016
Accepted for publication 7 June 2016
Published 13 July 2016

Abstract

We report the generation of coherent water-window soft x-ray harmonics in a neon-filled semi-infinite gas cell driven by a femtosecond multi-mJ mid-infrared optical parametric chirped-pulse amplification (OPCPA) system at a 1 kHz repetition rate. The cutoff energy was extended to ~450 eV with a 2.1 μm driver wavelength and a photon flux of $\sim 1.5 \times 10^6$ photons/s/1% bandwidth was obtained at 350 eV. A comparable photon flux of $\sim 1.0 \times 10^6$ photons/s/1% bandwidth was observed at the nitrogen K-edge of 410 eV. This is the first demonstration of water-window harmonic generation up to the nitrogen K-edge from a kHz OPCPA system. Finally, this system is suitable for time-resolved soft x-ray near-edge absorption spectroscopy. Further scaling of the driving pulse's energy and repetition rate is feasible due to the availability of high-power picosecond Yb-doped pump laser technologies, thereby enabling ultrafast, tabletop water-window x-ray imaging.

Keywords: x-rays, soft x-rays, ultrafast lasers, nitrogen K-edge, high harmonic generation, water window

(Some figures may appear in colour only in the online journal)

1. Introduction

Recent progress in ultrafast high-peak-power laser systems has allowed for significant advancements in the field of nonlinear optics. This is particularly true of the extreme nonlinear optical phenomenon known as high-harmonic generation (HHG), in which an atom is tunnel-ionized at high laser intensities of 10^{13}–10^{14} W cm^{-2} and the electron is accelerated by the rapidly oscillating optical field and eventually recombines with its parent ion [1]. This process can be used to generate coherent photons in energy ranges, extending into the soft x-ray regime, that are not otherwise achievable from a tabletop system, resulting in coherent short-wavelength harmonic emission over multiple half cycles of the driving laser field. As the emitted photon energy is proportional to the squared drive wavelength, mid-infrared (MIR) laser pulses have enabled energies in the soft x-ray regime up to ≈1.5 keV via HHG [2] from a tabletop system. Synchrotrons and free electron lasers (FEL's) are capable of

[5] G J Stein and P D Keathley contributed equally to this work.

Original content from this work may be used under the terms of the Creative Commons Attribution 3.0 licence. Any further distribution of this work must maintain attribution to the author(s) and the title of the work, journal citation and DOI.

 © 2016 IOP Publishing Ltd Printed in the UK

producing coherent high-flux photons at high energies up to soft and hard x-ray regions as well, however such systems based on an accelerator are extremely large and expensive. Furthermore, while a FEL can generate few femtosecond x-ray pulses, they are not easily synchronized with optical pulses for studying temporal dynamics [3]. Current state-of-the-art techniques for synchronizing x-ray FEL pulses and optical pulses can achieve a timing jitter down to a few fs, however this pales in comparison to HHG based systems where attosecond studies are routinely performed, and timing jitter down to 20 as rms is attainable [4]. Though FELs have the ability to generate enormous photon fluxes, HHG has the unique capacity to open new frontiers in time-resolved absorption spectroscopy and attosecond science in the soft x-ray regime.

The potential applications of this source are many, as having high energy (and thereby short-wavelength) photons opens the door to imaging at unprecedented spatial and temporal resolutions and at interesting energy ranges. In particular, there is considerable interest in generating photons within the soft x-ray energy water window, a region above the 284 eV carbon K-edge, within which atoms of carbon become highly absorptive, and below 543 eV oxygen K-edge, within which water molecules are still transparent. A high-flux, coherent source capable of generating energy in the water window is capable of imaging biological samples (whose primary components include carbon) [5, 6] or performing near-edge absorption spectroscopy [7]. A table-top, HHG based water window source will enable the study of cellular processes at otherwise unattainable time-scales or to perform simultaneous imaging and spectroscopy in a conventional laboratory setting. A similar spectral feature exists at 410 eV in nitrogen, which is a primary component of DNA, one of the building blocks of life. This could allow for the selective imaging or absorption spectroscopy [8] of DNA and RNA within a cell, further motivating the development of a high-harmonic source capable of producing photons above $\approx$400 eV.

Despite the promise of this technique, low photon fluxes from HHG have been the main challenge facing applications such as microscopy and spectroscopy. Since the single-atom efficiency of HHG scales unfavorably with the drive wavelength, scaling of soft x-ray HHG from a MIR driver is possible only with good phase-matching in high gas pressures [9]. Phase matching is also difficult to achieve for long driving wavelengths, like MIR, because of strong plasma effects which invariably occur during the macroscopic propagation [10]. There has been a dedicated effort to encourage phase-matching by modifying the propagation geometry of the driver pulse, often by confining it to a gas-filled cylindrical capillary [11]. However, the existence of strong filamentation at high pressures (typically 1–40 bar) for optimal HHG conversion introduces complicated phase matching mechanisms that are not yet clearly understood [2]. Instead, discussions of the propagation geometry are motivated by gas pressure handling, which has proven to be of equal or greater concern.

While increasing the conversion efficiency of HHG for a fixed laser energy is quite challenging, the onus for increasing the HHG photon flux is on the laser engineering community, motivating the development of MIR laser sources which are of increasingly high repetition rates yet still maintain the peak intensities necessary for reaching the photon energies of interest. Our optical parametric chirped-pulse amplification (OPCPA) system, capable of producing 2.1 μm, 32 fs, multi-mJ pulses at a 1 kHz repetition rate, is at the forefront of technologies capable of satisfying this constraint.

In this paper, we report water-window HHG in a neon-filled, semi-infinite gas cell with a high harmonic cutoff of nearly 450 eV and a photon flux of $\approx 10^6$ photons/s/1% bandwidth at the nitrogen edge of 410 eV. Furthermore, we support all of our results with a numerical study, which shows good agreement with the experimental data. Recent demonstrations have shown that cryogenic Yb:YAG pump sources are ideal for generating pulses 1–10 ps (suitable for OPCPA technology) and can be scaled to average powers of up to 250 W at a repetition rate of 100 kHz [12], and 758 W at 50 MHz [13]. It is feasible that the repetition rate of our present pump scheme can be scaled to a rate of 10–100 kHz. Making conservative estimates of our source spot size and beam divergence, switching to a 100 kHz source would yield a brilliance between 10^8 and 10^9 photons/(s $\times$ 0.1%BW $\times$ μm^2 $\times$ sr) at the nitrogen k-edge if all other parameters are left fixed. Utilizing conventional soft x-ray optics, such a peak brilliance is enough to create a table-top soft x-ray imaging system [14] with a tunable wavelength range and/or sub-fs timing resolution. Furthermore, utilization of the spatial coherence of HHG is possible, further decreasing the necessary flux for imaging [15].

There have been a few recent demonstrations of water-window soft x-ray HHG using optical parametric amplifiers (OPA's) at kHz repetition rates that are not scalable to much more than the few-watt level [16], due to the limited average power available from Ti:Sapphire laser systems. However our OPCPA-based driving laser source has the potential for further energy and average power scaling due to the high average powers available from picosecond Yb:YAG laser systems and energy scalability provided by the OPCPA architecture. Though scaling provides its own challenges (thermal effects can arise above 100 W and the pulse compression setup may become more difficult), these are engineering challenges and do not present any theoretical difficulty. This provides our OPCPA based soft x-ray source the potential for further increasing the high harmonic flux to levels which are unachievable using Ti:Sapphire pumped OPAs.

2. Experimental setup

Our experimental setup consisted of a custom, home-made multi-mJ 1 kHz 2.1 μm OPCPA system discussed at length in [17, 18] driving a semi-infinite gas cell as a HHG target, which is the combination of a gas cell and a hollow capillary, followed by an x-ray filter assembly, a grazing-incidence

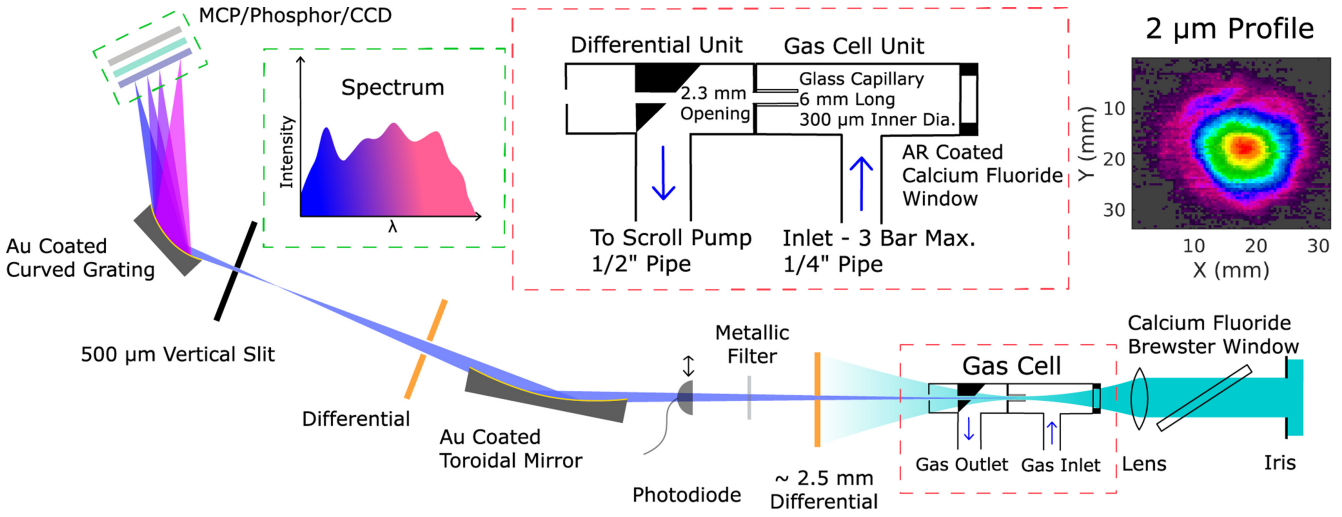

Figure 1. Experimental setup of the HHG generation and characterization apparatus.

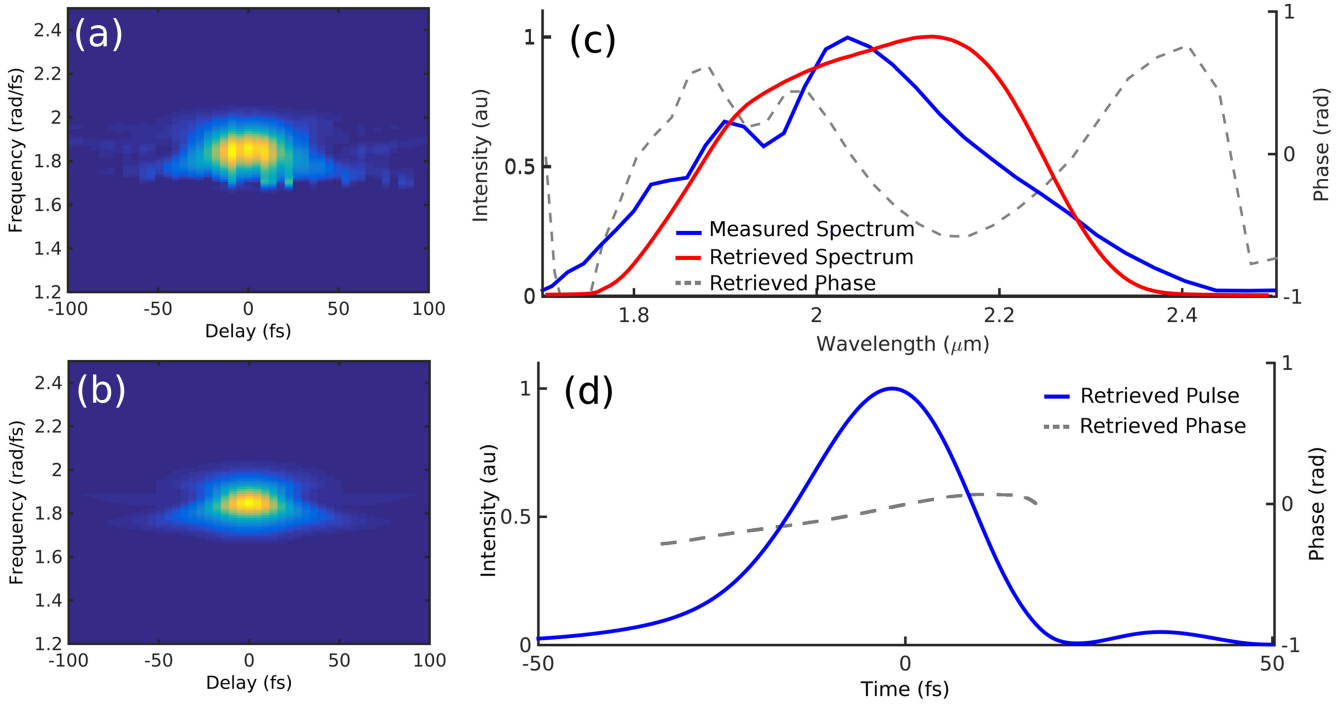

Figure 2. FROG measurements for the laser source. (a) The measured spectrogram. (b) The retrieved spectrogram. (c) The measured (blue) and retrieved spectra (red), along with the retrieved phase (dashed gray). (d) The retrieved time-domain pulse envelope (blue) and pulse phase (dashed gray).

toroidal mirror and a 1 m radius of curvature Rowland circle spectrometer (McPherson Model 248/310) for measuring the high-harmonic spectra. A schematic of the experimental apparatus is shown in figure 1, and each component is discussed in greater detail in the following paragraphs.

The evolution and performance of our driving laser source has been demonstrated a number of times [17, 19, 20]. The most recent upgrade includes a picosecond hybrid Yb-doped amplifier as the pump laser of an OPCPA [18], which provides highly stable pointing stability over many hours. The frequency-resolved optical gating (FROG) measurement of the OPCPA output pumped by this Yb-doped amplifier is shown in figure 2. We also rely on a Fastlite DAZZLER pulse shaper to compensate for the differences in dispersion between the FROG measurement and the detection chamber, so that detected pulse can most accurately match that which we use for the experiment.

The figure shows a pulse duration of ≈26 fs at a central wavelength of 2.06 μm, corresponding to a roughly ≈3.8 cycle pulse. However, during the HHG measurements, a slightly narrower bandwidth was used, corresponding to a pulse duration of 32 fs, or 4.5 optical cycles. The maximum energy from the OPCPA system in this configuration is 3.5 mJ before compression, but, as a safety margin, we

operate at 2.5 mJ before compression (2.0 mJ available inside the chamber, after compressor and routing optics).

The 2.1 μm beam was set to a diameter of approximately $\approx$10 mm in $1/e^2$ at the chamber entrance, and an image of the beam profile is shown in figure 1. The actual spot size was slightly decreased for optimal HHG using an adjustable iris. The chamber beam entrance was formed using a 6 mm thick calcium fluoride window at Brewster's angle for maximum transmission. Inside of the vacuum chamber, the beam was focused using two, stacked, anti-reflection-coated CaF_2 lenses, each having a focal length of 750 mm, effectively forming a lens with a 375 mm focal length. This focal length was found to be optimal for HHG in Ne after we tested with several focal lengths.

Having known that the phase matching of 2.1 μm driven HHG in Ne happens at >1 bar [9, 21], we designed a semi-infinite gas cell containing a hollow capillary that can handle high pressure with good differential pumping towards the soft x-ray spectrometer, which was modified from our previous work [21]. The gas cell/hollow capillary target, shown as the right insert in figure 1 was constructed with an AR-coated CaF_2 window to contain the gas at the entrance. The interior of the gas cell was simply a small, hollow chamber at the center of a tee, with the beam input on one side, the glass capillary on the other, and the gas supply inlet attached at a 90° angle. The propagation length from the inside of the entrance window of the gas cell unit to the entrance of the capillary was approximately 10 cm. The pressure of the gas line was measured just outside of the chamber wall using a Pirani/piezo pressure gauge (MKS 910, MKS Instruments) with an upper limit of 2.0 bar. For pressures exceeding this limit, the regulator gauge was used. It was verified that the regulator gauge matched that of the MKS 910 gauge to within 5%.

The 6 mm long glass capillary had an inner diameter of 300 μm, sealed from the surrounding chamber system using a rubber o-ring. The capillary was followed by a differential stage connected to a 35 m^3/h scroll pump through a $1/2''$ pipe. The differential stage was crucial in limiting the gas load supplied to the surrounding chamber, allowing for up to 3 bar pressure to be supplied to the gas cell without damaging the turbomolecular pump. Furthermore, the differential stage limited reabsorption of the HHG during propagation to the spectrometer.

The 2.1 μm beam was focused just inside the entrance of the hollow capillary for optimal generation of high-harmonics. From here, the high-harmonic beam was sent through the differential stage of the gas cell, and a 2.5 mm diameter hole serving as a second differential between the main generation chamber and the toroidal mirror/filter chamber.

Near the entrance of the toroidal mirror/filter chamber, filters and metallic-coated x-ray photodiodes were used for optimizing the HHG signal and calibrating the HHG energy spectrum and flux. The photodiodes provided a much faster feedback mechanism for monitoring HHG flux than the soft x-ray spectrometer, and did not have the added complication of spatial alignment to the narrow entrance slit of the spectrometer. Due to leakage of parasitic generation (likely of UV and deep UV light), it was necessary to ensure that only the proper HHG signal was optimized during beam alignment to the target. This was achieved by using a wave plate capable of adding a slight ellipticity to the drive beam. At each step of the optimization process, it was verified with the waveplate that the signal was maximized with linear polarization and rapidly diminished with even a slight ellipticity, a well-known property of HHG.

Just after the filter assembly a gold coated toroidal mirror at approximately 86° grazing incidence was used to focus the HHG near the spectrometer slit. The exact angle was tuned for minimum astigmatism at focus, and it was confirmed during measurement that the HHG was focused to a spot smaller than the slit opening, which was set to $\approx$500 μm, the maximum width. For the spectral measurements in the water-window region, a gold-coated cylindrical grating with 2400 grooves/mm was used to image the spectrum onto the Rowland circle, and it was detected with a microchannel plate/ phosphor screen/ CCD stack. To improve the signal to noise ratio of the detector, the CCD was cooled to −40 °C, and binning was used to integrate over only x-ray-exposed rows of the CCD array. This ensured an adequately low noise floor in the measurements.

3. Experimental results

We performed soft x-ray HHG experiments in Ar and Ne gases using the 2.1 μm driver. First, measurements on HHG in Ar were conducted to show that our system was functioning correctly, since we have previously demonstrated high-flux, soft x-ray HHG in Ar at 60–200 eV [17] using a similar experimental setup. Consistent with this previous work, the maximum flux occurs for roughly 200 mbar of Ar and required limiting our pulse energy to roughly 1 mJ and tuning the pressure to avoid detrimental plasma effects. This corresponds to a beam waist of $\approx$55 μm and a peak intensity of $\approx 6 \times 10^{14}$ W cm^{-2}. Furthermore, we observed that the location of the focus was deep into the capillary, so that the maximum intensity of the beam occurred within 1–2 mm of the vacuum region at the output. Physically, it seems this condition helps to minimize the reabsorption of soft x-ray harmonics and the the plasma defocusing of the pulses as they propagate through the gas. The HHG measurements for Ar can be found in the leftmost plot in figure 3. In order to confirm that our spectrometer was properly calibrated, two different sets of filters were used: (1) a 1 μm thick carbon filter and (2) a 1 μm thick carbon filter with an additional 500 nm thick boron filter. The transmission curves for these filter sets can be found in the bottom left plot of figure 3. We observed the boron K-edge at 188 eV. The slope of the edge is not steep due to a low resolution of the soft x-ray spectrometer with the maximum opening of the slit. In addition, the cutoff energy is observed to be around 200 eV with only the carbon filter, consistent with previous studies [17, 21].

The results on HHG in Ne were collected with 1.35 mJ pulses, corresponding to a peak focal intensity of

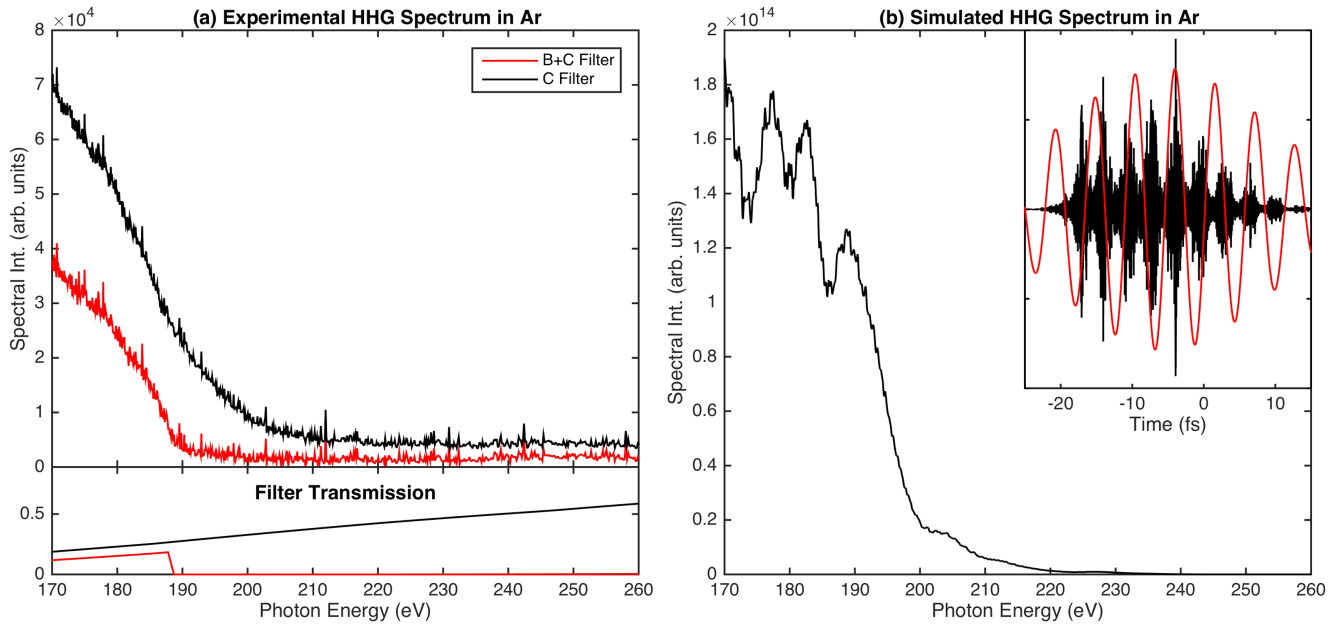

Figure 3. Experimental (left) and simulated (right) spectra for high harmonic generation in 0.2 bar of Ar for laser parameters given in the text. The lower photon energy is bounded by 170 eV because of the configuration of the spectrometer. The experimental spectra are taken using filters of boron and carbon, whose response curves are shown on the bottom left, so that we may visualize the boron K-edge at 188 eV. Notice the similarity, particularly in cutoff energy, between the experimental and simulated spectra. The sharper appearance of the simulated spectrum with respect to its experimental counterpart is a result of averaging; each experimental result includes thousands of shots. The inset in the simulated plot (right) shows the temporal profile of the simulated HHG pulses (black curve) along with the electric field of the 2 μm pulse (red curve).

$\approx 1.2 \times 10^{15}$ W cm^{-2}, and at a gas pressure of 1.5 bar, which was experimentally observed to maximize the signal on our calibrated, titanium/carbon (Ti/C) coated photodiode (AXUV100Ti-C2 from IRD Inc.). The pulse energy used is less than the peak energy available as it was necessary to adjust the entrance iris when optimizing for HHG conversion efficiency. As with the Ar results, the spectra for Ne were collected in the presence of two different filters: one comprised of 1 μm of carbon (black) and one of 500 nm of titanium (red). In addition to obstructing the driver pulse, the spectral responses of the filters also have a rather profound effect on the spectra. The corresponding response curves are shown in the bottom left plot of figure 4. Each spectrum was accumulated over a 100 s integration time.

With the carbon filter, we clearly observed the carbon K-edge at 284 eV, demonstrating that the HHG in Ne reached the water-window soft x-ray region. One might notice that the Carbon K-edge is expected to be extremely sharp, though the measured profile is relatively smooth. While this is in part due to the spectrometer resolution, it is an interesting result that is consistent with what others have observed [22].

The full spectrum can be observed as the red curve in the left plot in figure 4, in which the beam is filtered by a 500 nm titanium filter. The spectrum shows a high harmonic cutoff of roughly 450 eV, which is not only well within the water window but also above the nitrogen K-edge at 410 eV. However, the spectral dip which occurs surrounding 284 eV is indicative of a small amount of carbon contamination in the system. The appearance of carbon is common, if not unavoidable, and roughly totals to only about a 50 nm thick film over the course of the soft x-ray beam's propagation. Such contamination features can be observed in other high energy HHG results, where the effects are even more severe [9].

Even in the presence of carbon, it is clear that the peak of the spectrum occurs at around 350 eV. An average current of $\approx$18 pA was measured on the Ti/C photodiode, corresponding to a photon flux of $\approx 1.5 \times 10^6$ photons/s/1% bandwidth at the peak energy of 350 eV and $\approx 1.0 \times 10^6$ photons/s/1% bandwidth at the nitrogen edge at 410 eV. Since our beam has to pass through a 2.5 mm diameter aperture between the gas cell and the photodiode, we can determine that our beam divergence is $< 6.25 \times 10^{-3}$ sr, and that the generated beam has a brilliance between 10^6 and 10^7 photons/(s $\times$ 0.1% BW $\times$ μm^2 $\times$ sr). The measured flux is comparable or slightly lower than previous reports in the water window range [9, 16] while the calibration methods are all different. The corresponding HHG conversion efficiency into 1% bandwidth is as low as 10^{-12}–10^{-11}. We believe this can be further increased by optimizing the gas cell geometry considering higher conversion efficiencies reported by other groups. Nevertheless, our measurements demonstrate the water-window HHG up to the nitrogen edge driven by an energy and power scalable kHz MIR OPCPA system, for the first time.

4. Modeling high harmonic generation

4.1. Theory for simulations

In addition to the experimental results, we use a simulation code, written in MATLAB, to further study the generation

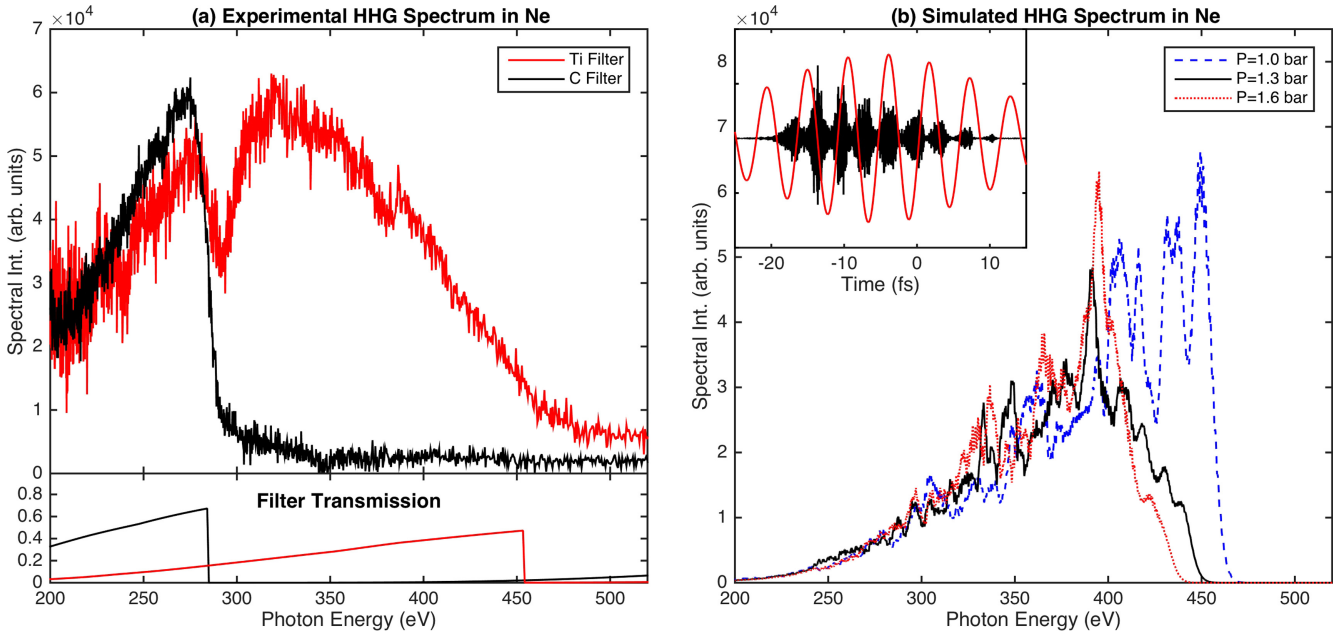

Figure 4. Experimental (left) and simulated (right) spectra for high harmonic generation in 1.3 bar of Ne gas for laser parameters given in the text. The carbon K-edge at 284 eV is clearly visible and the spectrum collected with the titanium filter shows that we have significant flux within the high harmonic 'water-window' with a cutoff of roughly 450 eV. The filter transmission curves of both the titanium and carbon filters are shown in the panel beneath the experimental data (left). These results are supported by our simulations. In particular, we include three different simulations, at pressures of 1.0, 1.3 and 1.6 bar, showing the effect of changing the gas pressure inside the capillary. Notice that increasing gas pressure results in a lower high harmonic cutoff as stronger plasma defocusing limits the maximum intensity of the beam. The result for $P = 1.3$ bar most closely matches the experiment. In addition, no metallic filters have been added to the simulation results to emphasize how near to the titanium edge the spectral cutoff occurs. The inset (right) shows the temporal profile of the resultant HHG pulses (black curve) along with the electric field of the 2 μm driving pulse (red curve) for a pressure of 1.3 bar.

process based on the three-step model [1] and 3D nonlinear pulse propagation [10]. The simulation code relies on the popular split-step Fourier technique [23], in which the linear and nonlinear contributions to the propagation equation are calculated and applied separately. In addition, the evolution of the macroscopic pulse is calculated independently from the HHG. For propagation of the driver pulse we follow the model employed in [10, 24, 25]:

$$\frac{\partial E}{\partial z} = \frac{\mathrm{i}}{2k}\nabla_\perp^2 E + \mathrm{i}\frac{k}{2}n_2\epsilon_0 c|E|^2 E - \frac{1}{2c}\int_{-\infty}^{\tau}\omega_\mathrm{p}^2 E\,\mathrm{d}\tau' - \frac{I_\mathrm{p}}{2c\epsilon\mathrm{Re}(E)^2}\frac{\partial\rho}{\partial\tau}E. \quad (1)$$

The first term on the right side of the equation describes the linear dispersion of the pulse. Since the pulses are restricted to a radially symmetric domain, and are therefore parameterized in terms of r, the Laplacian is solved in the spectral domain by way of a Hankel transform [26]. The second term, given in terms of the Kerr coefficient n_2, is the self-focusing and self-phase modulation term, solved using the well-known Runge–Kutta method [27]. The remaining two terms are the contributions which come about in the presence of plasma, represented by the plasma density ρ; the first term is a function of the squared plasma frequency ω_p^2 and the second, the loss of energy from the ionization process, is given in terms of the ionization potential I_p. The generated plasma is calculated using the Ammosov–Delone–Krainov ionization rate [28]. Finally, though the effect of the capillary boundary has been included in the simulation, it is presence only nominally effects the propagation, reinforcing the idea that the hollow glass core serves mostly to support the differential gas pressure.

Once the macroscopic pulse propagation is complete (for a particular time-step), the high harmonic response can be calculated using the well-known three-step-model [1]. The calculation is also augmented by quantitative rescattering theory [29], which allows us to include atomic spectral response curves (via the recombination amplitude [30]) that can be determined from experimental data. Combined with the equation above, this simulation model is sufficient for accurate simulations of HHG in a host of confining geometries, including free-space, cylindrical hollow capillaries, and high-pressure gas cells, the latter being used in this experiment.

Our simulation code, which has already been successfully employed to simulate the generation of high harmonics in Ar gas [17], has been modified to match the current experimental setup, using the parameters descried in the previous sections. The results, reproduced in the right plot of figure 3, show the effectiveness of the code in reproducing experimental results. In particular, notice that this the high-harmonic cutoff energies are in very good agreement, hovering just above 200 eV, and both spectra have roughly similar profiles in the region just beneath the cutoff. The temporal profile of the high harmonic pulse, calculated from the simulations, is also included. Otherwise extremely

difficult to obtain, this profile shows that the generation process expectedly results in a train of attosecond pulses.

4.2. Simulated HHG spectra from neon

In an effort to understand our results from the previous section, this model was modified to support generation in Ne gas. In close agreement with the experimental parameters, the simulated laser pulses have $\tau = 32$ fs, a focused beam waist of 45 μm and an energy of 1.35 mJ, thereby matching the peak intensity of roughly 1.2×10^{15} W cm^{-2}. In addition, the gas pressure inside the semi-infinite cell, of length 5 mm, is set to $P = 1.3$ bar and is given a smooth Lorentzian tail at the output (where the beam is focused) to avoid sharp discontinuities. Due to physical constraints, it was not possible to measure the gas pressure inside of the gas cell housing, but, rather, at a location outside of the vacuum chamber. Thus, the pressure inside of the gas cell is slightly less than the measured value. Our simulations indicate that a pressure of 1.3 bar yields the best match to the measured spectra given the laser parameters cited. This result can be compared to spectra for 1.0 and 1.6 bar of Ne, which are also shown in figure 4(b).

The inset of figure 4(b) shows the simulated high harmonic spectrum and the corresponding temporal response. As expected from the experimental results, the high-harmonic spectrum is effectively bounded below by 250 eV and above by about 440 eV, which is the high harmonic cutoff energy. At first glance, the agreement between the simulated and experimental spectral shape is potentially difficult to see, since the filters are not included in the simulation and their spectral features, particularly that of the carbon edge at 284 eV, are missing. In addition, the experimental spectrum appears to peak near its center around 350 eV whereas the simulated spectrum continues to rise. However, small fluctuations in the laser energy, which is typical of systems like ours, results in a shift of the peak energy of the pulse. As such, the aggregate spectrum, which is integrated over many thousands of shots of different energies, cannot be directly matched to any one-shot spectrum, which is produced by the simulations. Attempting to reproduce the full spectrum with the simulations is computationally infeasible. Fortunately, the most significant features of the simulation results match those of the experiments, further supporting the efficacy of the model.

Consistent with the experimental observations, the simulated peak driver intensity occurs very near to the output of the gas cell. Since the high harmonic photons are generated within a very narrow region surrounding this peak intensity, phase matching of the conversion process does not play a significant role in determining the output flux. Enhancement of the flux through phase matching, which would require fine-tuning of a host of parameters over an extended distance, remains an elusive goal for the parameter regime of interest here. However, for our current approach, the key limitation to getting higher photon flux is gas handling. After the generation region, any gas causes attenuation of the flux through reabsorption of the high harmonic photons. As such, the creation of a more compact gas cell and better differential pumping mechanisms is a clear path forward to increasing the output flux.

5. Conclusion

We have generated and characterized HHG in the water window region using a 2.1 μm OPCPA system and a neon-filled, semi-infinite gas cell. Spectral characterization clearly demonstrates photons generated between the carbon K-edge at 284 eV and the cutoff energy of around 450 eV. By using a calibrated Ti/C photodiode, it was possible to determine that a flux of $\approx 10^6$ photons/s/1% bandwidth was generated around 410 eV, the nitrogen K-edge. To supplement these measurements, simulated spectra were generated using a range of parameters consistent with our experimental conditions. These simulations show quantitatively good agreement with the measurement experimental cutoff energies and overall spectral ranges.

Given that such OPCPA technology is scalable in terms of both energy and average power, and has many advantages when engineering synthesized pulse waveforms [31] for potentially boosting HHG efficiency [32], we feel it will prove to be useful for extending the limits of HHG based sources. In fact, by increasing the system repetition rate to 100 kHz, which is within engineering limitations for the cryogenic Yb:YAG pump technology used, one could scale the HHG brilliance to between 10^8 and 10^9 photons/(s $\times$ 0.1%BW $\times$ μm^2 $\times$ sr) at the nitrogen k-edge keeping all else unchanged, making the system's flux comparable to laser plasma sources for water window imaging [14]. As opposed to plasma sources which generate flux only on fixed atomic lines, an HHG source has the added advantages of wavelength tunability and/or sub-fs time resolution. In general, the design of high-pressure gas cells and the laser performance are keys to further scaling of soft x-ray HHG flux as well as improving the stability and reliability of table-top soft x-ray HHG sources for applications to time-resolved imaging and spectroscopy in the full water-window region.

Acknowledgments

This work was supported by the AFOSR (FA9550-12-1-0499, FA9550-12-1-0080, and FA9550-14-1-0255), the Center for Free-Electron Laser Science, DESY, Germany, and the excellence cluster 'The Hamburg Centre for Ultrafast ImagingStructure, Dynamics and Control of Matter at the Atomic Scale' of the Deutsche Forschungsgemeinschaft. C-L Chang acknowledges the Ministry of Science and Technology in Taiwan for the Postdoctoral Research Abroad Program NSC 102-2917-I-564-026. H K Liang acknowledges financial support from Singapore Institute of Manufacturing Technology (SIMT/14-110023) and Agency for Science, Technology and Research (A*STAR), Singapore. J P Siqueira acknowledges FAPESP (2012/22102-7) for the funding support through the program BEPE, Brazil. G J Stein, P D Keathley

and P Krogen all acknowledge support by a NDSEG Graduate Fellowship.

References

[1] Lewenstein M, Balcou P, Ivanov M Y, L'Huillier A and Corkum P B 1994 *Phys. Rev.* A **49** 2117–32
[2] Popmintchev T *et al* 2012 *Science* **336** 1287–91
[3] Harmand M *et al* 2013 *Nat. Photon.* **7** 215–8
[4] Chini M, Mashiko H, Wang H, Chen S, Yun C, Scott S, Gilbertson S and Chang Z 2009 *Opt. Express* **17** 21459–64
[5] Weiß D, Schneider G, Niemann B, Guttmann P, Rudolph D and Schmahl G 2000 *Ultramicroscopy* **84** 185–97
[6] Larabell C A and Le Gros M A 2004 *Mol. Biol. Cell* **15** 957–62
[7] Hahner G 2006 *Chem. Soc. Rev.* **35** 1244–55
[8] Kirtley S M, Mullins O C, Chen J, van Elp J, George S J, Chen C, O'Halloran T and Cramer S P 1992 *Biochimica Biophys. Acta (BBA)—Gene Struct. Expression* **1132** 249–54
[9] Chen M C, Arpin P, Popmintchev T, Gerrity M, Zhang B, Seaberg M, Popmintchev D, Murnane M M and Kapteyn H C 2010 *Phys. Rev. Lett.* **105** 173901
[10] Lai C J and Kärtner F X 2011 *Opt. Express* **19** 22377–87
[11] Jin C, Stein G J, Hong K H and Lin C D 2015 *Phys. Rev. Lett.* **115** 043901
[12] Zapata L E, Reichert F, Hemmer M and Kärtner F X 2016 *Opt. Lett.* **41** 492
[13] Brown D C, Singley J M, Kowalewski K, Guelzow J and Vitali V 2010 *Opt. Express* **18** 24770
[14] Benk M, Bergmann K, Schäfer D and Wilhein T 2008 *Opt. Lett.* **33** 2359
[15] Sandberg R L *et al* 2008 *Proc. Natl Acad. Sci.* **105** 24–7
[16] Cousin S L, Silva F, Teichmann S, Hemmer M, Buades B and Biegert J 2014 *Opt. Lett.* **39** 5383–6
[17] Hong K H, Lai C J, Siqueira J P, Krogen P R, Moses J, Chang C L, Stein G J, Zapata L E and Kärtner F X 2014 *Opt. Lett.* **39** 3145–8
[18] Chang C L *et al* 2015 *Opt. Express* **23** 10132
[19] Moses J, Manzoni C, Huang S W, Cerullo G and Kaertner F X 2009 *Opt. Express* **17** 5540–55
[20] Hong K H, Huang S W, Moses J, Fu X, Lai C J, Cirmi G, Sell A, Granados E, Keathley P and Kärtner F X 2011 *Opt. Express* **19** 15538–48
[21] Lai C J *et al* 2015 *J. Opt.* **17** 094009
[22] Takahashi E J, Kanai T, Ishikawa K L, Nabekawa Y and Midorikawa K 2008 *Phys. Rev. Lett.* **101** 253901
[23] Agrawal G P 2007 *Nonlinear Fiber Optics* (New York: Academic)
[24] Geissler M, Tempea G, Scrinzi A, Schnürer M, Krausz F and Brabec T 1999 *Phys. Rev. Lett.* **83** 2930–3
[25] Hong K H, Lai C J, Gkortsas V M, Huang S W, Moses J, Granados E, Bhardwaj S and Kärtner F X 2012 *Phys. Rev.* A **86** 043412
[26] Yu L, Huang M, Chen M, Chen W, Huang W and Zhu Z 1998 *Opt. Lett.* **23** 409–11
[27] Press W H, Teukolsky S A, Vetterling W T and Flannery B P 2007 *Numerical Recipes: The Art of Scientific Computing* (Cambridge: Cambridge University Press)
[28] Ammosov M V, Delone N B and Krainov V P 1986 *J. Exp. Theor. Phys.* **64** 1191
[29] Le A T, Lucchese R R, Tonzani S, Morishita T and Lin C D 2009 *Phys. Rev.* A **80** 013401
[30] Bhardwaj S, Son S K, Hong K H, Lai C J, Kärtner F X and Santra R 2013 *Phys. Rev.* A **88** 053405
[31] Huang S W *et al* 2011 *Nat. Photon.* **5** 475–9
[32] Jin C, Wang G, Wei H, Le A T and Lin C D 2014 *Nat. Commun.* **5** 4003